




Molecular characterization of histopathological ependymoma variants

Julia E. Neumann¹ · Michael Spohn^{2,15} · Denise Obrecht³ · Martin Mynarek³ · Christian Thomas⁴ ·
Martin Hasselblatt⁴ · Mario M. Dorostkar^{5,6} · Annika K. Wefers^{7,8,9} · Stephan Frank¹⁰ · Camelia-Maria Monoranu¹¹ ·
Arend Koch¹² · Hendrik Witt^{9,13,14} · Marcel Kool^{9,13} · Kristian W. Pajtler^{9,13,14} · Stefan Rutkowski³ · Markus Glatzel¹ ·
Ulrich Schüller^{1,3,15} 

Received: 8 August 2019 / Revised: 15 October 2019 / Accepted: 27 October 2019 / Published online: 2 November 2019
© Springer-Verlag GmbH Germany, part of Springer Nature 2019

Abstract

According to the WHO classification, ependymal tumors are classified as subependymomas, myxopapillary ependymomas, classic ependymomas, anaplastic ependymomas, and *RELA*-fusion-positive ependymomas (*RELA*-EPN). Among classic ependymomas, the WHO defines rare histological variants, i.e., the clear cell, papillary, and tancytic ependymoma. In parallel, global DNA methylation patterns distinguish nine molecular groups, some of which tightly overlap with histopathological subgroups. However, the match of the aforementioned histological variants to DNA methylation classes remains unclear. We analyzed histomorphology, clinical parameters, and global DNA methylation of tumors with the initial histological diagnoses of tancytic ($n = 12$), clear cell ($n = 14$), or papillary ependymoma ($n = 19$). Forty percent of these tumors did not match to the epigenetic profile of ependymomas, using a previously published DNA methylation-based classifier for brain tumors. Instead, they were classified as low-grade glioma ($n = 3$), plexus tumor ($n = 2$), CNS high-grade neuroepithelial tumor with *MN1* alteration ($n = 2$), papillary tumor of the pineal region ($n = 2$), neurocytoma ($n = 1$), or did not match to any known brain tumor methylation class ($n = 8$). Overall, integrated diagnosis had to be changed in 35.6% of cases as compared to the initial diagnosis. Among the tumors molecularly classified as ependymoma (27/45 cases), tancytic ependymomas were mostly located in the spine (5/7 cases) and matched to spinal or myxopapillary ependymoma. 6/8 clear cell ependymomas were found supratentorially and fell into the methylation class of *RELA*-EPN. Papillary ependymomas with a positive ependymoma match (12/19 cases) showed either a “papillary” ($n = 5$), a “trabecular” ($n = 1$), or a “pseudo-papillary” ($n = 6$) growth pattern. The papillary growth pattern was strongly associated with the methylation class B of posterior fossa ependymoma (PFB, 5/5 cases) and tumors displayed DNA methylation sites that were significantly different when compared to PFB ependymomas without papillary growth. Tumors with pseudo-papillary histology matched to the methylation class of myxopapillary ependymoma (4/6 cases), whereas the trabecular case was anatomically and molecularly a spinal ependymoma. Our results show that the diagnosis of histological ependymoma variants is challenging and epigenetic profiles may improve diagnostic accuracy of these cases. Whereas clear cell and papillary ependymomas display correlations between localization, histology, and methylation, tancytic ependymoma does not represent a molecularly distinct subgroup.

Keywords Ependymoma · Tancytic · Clear cell · Papillary · *RELA* · PFB

Introduction

Ependymal tumors are neuroepithelial neoplasms that commonly grow attached to ventricles or to the central canal of the spinal cord. They predominantly occur in children, but may also affect adults. Tumors may metastasize and display a decreasing survival rate related to younger age. In particular, a large study combining ependymomas with choroid plexus tumors ($n = 1233$) found a survival rate of only 42.4% and 55.3% 5 years after diagnosis for patients

Electronic supplementary material The online version of this article (<https://doi.org/10.1007/s00401-019-02090-0>) contains supplementary material, which is available to authorized users.

✉ Julia E. Neumann
ju.neumann@uke.de

✉ Ulrich Schüller
u.schueller@uke.de

Extended author information available on the last page of the article

diagnosed below the age of 1 year or aged 1–4, respectively [11]. In a more recent clinical trial, the 10 year overall survival in children with ependymoma (aged ≤ 3 , $n = 54$) was at around 60% [32]. Based on the current WHO classification (2016), ependymal tumors can be classified as subependymomas (WHO°I), myxopapillary ependymomas (WHO°I), classic ependymomas (WHO°II), anaplastic ependymomas (WHO°III), and *RELA*-fusion-positive ependymomas (WHO°II/III). Whereas myxopapillary ependymomas typically occur in the cauda equina and *RELA*-fusion-positive ependymomas grow supratentorially, subependymomas, classic ependymomas, and anaplastic ependymomas may all arise from supratentorial, infratentorial, and spinal origins. In addition, the vast majority of ependymomas share histological hallmarks, such as perivascular pseudorosettes, ependymal linings, and, less frequently, true ependymal rosettes, independent of their anatomical localization. However, patients of different age groups tend to develop ependymomas in different locations. Whereas more than 90% of the tumors occurring in childhood are located in the posterior fossa, ependymomas during adulthood are mostly arising in the spinal cord [15].

With the advent of broad molecular analyses, the hypothesis that ependymomas from different localizations are most likely distinct entities was strengthened. For example, mutations in *NF2* have been detected as an aberration of spinal ependymoma [8], whereas *C11orf95-RELA* gene fusions exclusively occur in supratentorial ependymomas [24]. In 2015, a landmark paper by Pajtler and colleagues used global DNA methylation to distinguish nine clinically different molecular groups of ependymoma, three in each of the three anatomical compartments [23]. Within this classification scheme, spinal ependymomas with *NF2* mutations established a separate methylation class within the nine groups. The same was true for supratentorial ependymomas with *RELA* fusions that were afterwards introduced as a novel, distinct entity into the latest update of the WHO classification for brain tumors in 2016 [18]. Global DNA methylation profiling is not only used to distinguish the nine different groups of ependymomas, but also to classify all different kinds of brain tumors [3]. The application of this technique allows the comparison of a tumor's DNA methylation profile to a large reference group of tumor methylation profiles and a matching to predefined "methylation classes", therefore, strengthening a suspected histopathological tumor diagnosis or suggesting appropriate differential diagnoses.

Among the group of classic ependymomas (WHO°II), the WHO classification defines three different histological variants: papillary ependymoma, tancytic ependymoma, and clear cell ependymoma [18]. Papillary ependymomas are described as rare tumors with finger-like projections that are lined by a single layer of cuboidal tumor cells. Papillae are lacking a basement membrane beneath the neuroepithelial

cells, which send fibrillary processes down to a vascular core similar to the architectural arrangement in a pseudorosette. Tancytic ependymomas display irregular fascicles of variable width and cell density and are reported to occur in the spinal cord, but may also grow intracranially [30, 31]. Pseudorosettes can be subtle, which is why the tumors may be mistaken for astrocytomas. Finally, clear cell ependymomas are described to exhibit perinuclear halos mimicking an oligodendroglioma phenotype or resembling central neurocytoma [19].

While most neuropathologists know how these variants are supposed to look like, many aspects remain unclear. Apart from the sparsely described histology, solid data on epidemiology, anatomical distribution, clinical outcome, and molecular biology are missing. In addition, although 500 ependymomas have been analyzed by Pajtler et al. via global DNA methylation [23], it remains elusive, which molecular subgroups such histological variants belong to.

We have analyzed a series of 45 ependymomas that had been diagnosed as papillary, tancytic, or clear cell ependymoma. To thoroughly characterize these ependymoma variants, we carefully re-evaluated histological features, gathered epidemiological and clinical data, and performed DNA methylation profiling.

Materials and methods

Human tissue

Biopsy material (FFPE samples) of tumors with a local and/or central diagnosis of any ependymoma variant within the years 1997–2018 was obtained from the tissue archives of various neuropathology units in Germany and Switzerland including cases that had been collected within the HIT-MED study cohort ($n = 17$). 42/45 cases included the histologic term "tancytic ependymoma", "papillary ependymoma", or "clear cell ependymoma" in the diagnostic top line. Three cases (cases 20, 24, 26) included the descriptive term "clear cell histology". All investigations were performed in accordance with local and national ethical rules regarding the use of patients' material and have, therefore, been performed in accordance with the ethical standards laid down in an appropriate version of the 1964 Declaration of Helsinki. Patients gave their informed consent prior to their inclusion in the study.

DNA methylation-based tumor analysis

DNA methylation data were generated using the Illumina HumanMethylation450 (450 k) or MethylationEPIC (850 k) array bead chips. Methylation analysis of ependymoma variants was performed using FFPE samples. To ensure a tumor

cell content of at least 80%, suitable tumor areas were microdissected, if necessary. Cases within the HIT-MED study cohort were either fresh frozen or FFPE samples. Following deparaffinization, DNA was extracted with the Maxwell[®] 16FFPE Plus LEV DNA Kit (Promega, Fitchburg, USA) and a Maxwell DNA extractor. About 250 ng of genomic DNA per sample were processed using the Illumina starter equipment (Illumina, San Diego) and the respective reagents. DNA quantification was performed with the Qubit[®] dsDNA BR Assay Kit (Thermo Fisher Scientific, Waltham, USA). Bisulfite conversion was done with the Zymo EZ Methylation Kit (Zymo Research Irvine, USA) followed by purification with Zymo DNA Clean Kit (Zymo Research Irvine, USA). DNA from FFPE tissue was treated with the Infinium HD FFPE Restore Kit prior to hybridization to the Infinium BeadChip (Illumina, San Diego). Subsequently, the bead chips were scanned by an iScan (Illumina, San Diego). The output data (.idat files) from the iScan reader were checked for general quality measures as indicated by the manufacturer.

DNA methylation-based classification, *t*-SNE analysis, and copy number plots

DNA methylation-based classification of brain tumors was performed using the publically available “classifier” tool, version v1.1b4 (<https://www.molecularneuropathology.org/mnp>, [3]), that currently recognizes 82 distinct CNS tumor entities. Calibrated methylation classifier scores < 0.5 were defined as “no match”. Scores ≥ 0.5 were considered in an integrated diagnostic setting, as described previously [4]. Raw idat files were loaded into the R environment (v3.5.2), and normalized and corrected for batch effects. Differentially methylated probes (DMP) were detected with ChAMP (v2.12.4) [20]. Samples from different array types (450 k or EPIC) were loaded separately and combined with the combineArrays function from the minfi package (v1.28.4) [1]. For visualization, pheatmap (v1.0.12) [16] was employed. *t*-distributed stochastic neighbor embedding (*t*-SNE) analysis was done as previously described [5]. For *t*-SNE plots, publicly available data from 82 defined brain tumor entities ($n = 2801$, [3], GEO accession number GSE90496) and from posterior fossa group B ependymomas ($n = 212$, [5], GEO accession number GSE117130) were included. Within the Cavalli data set [5], the cases GSM3271672, GSM3271667, GSM3271694, GSM3271693, GSM3271775, GSM3271656, GSM3271742, GSM3271688, GSM3271708, GSM3271837, and GSM3271672 were also present in the HIT study cohort and we analyzed. To avoid double cases, these data were excluded from analyses.

To obtain cumulated copy number variations (CNVs) per group, each sample was first analyzed separately with the ‘conumee’ package for R (v1.9.0) [13]. Afterwards,

the proportions per group were estimated by DNACopy (1.58.0) [21]. *t*-SNE and cumulated CNVs were visualized by ggplot2 (v3.1.1) [33].

Histology, immunohistochemistry, FISH, and gene fusion analyses

After DNA methylation-based tumor analysis, a histopathological review of all cases was performed by J.N. and U.S. as board-certified neuropathologists to find an integrated diagnosis. To this end, formalin-fixed and paraffin-embedded human tumor samples were H&E-, Astra-, or Alcian-stained according to standard protocols. Information on immunohistochemistry was taken from local or central reports if material was not available or done on an automated Ventana system using the following primary antibodies: anti-GFAP (DAKO, M0761, 1:200), anti-NFP (DAKO M0762, 1:400), anti-Brachyuri (R&D, BAF2085, 1:50), anti-OLIG2 (Millipore AB9610, 1:50), anti-H3K27me3 (Cell Signaling 9733, 1:50), anti-H3K27 M (Millipore MAB3303, 1:1000), anti-Synaptophysin (DAKO M7315, 1:500), anti-IDH1 (R132H, Histoviva DAH09, 1:20), anti-Keratin (Immunotech 1918, 1:400), anti-Vimentin (DAKO 0725, 1:200), rabbit anti-S100 (DAKO Z0311, 1:8000), anti-EMA (DAKO 0613, 1:200), anti-p53 (DAKO M7001, 1:800), anti-MAP2C (Sigma, M4403, 1:3000), anti-ATRX (HPA001906, 1:400), anti-CD34 (DAKO M7165, 1:100), anti-p65 (Cell Signaling 8242S, 1:2000), and anti-NeuN (Merck, MAB377, 1:25). *RELA-C11orf95* fusions were investigated using protocols and primers published elsewhere [24]. FISH analyses to detect alterations within *MNI* were performed using standard protocols and probes by Cytotest (CT-PAC112-100G).

Results

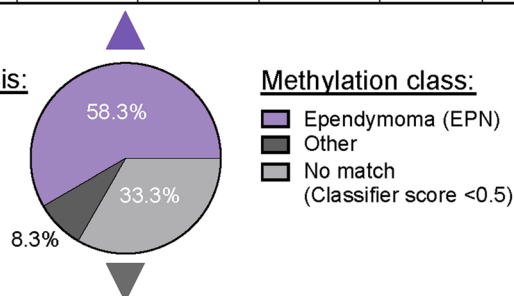
Tanycytic ependymoma

Histologically diagnosed tanycytic ependymoma cases ($n = 12$) had a median age of 34.5 years (range 10.4–80.7) with a female-to-male ratio of 2:1 (Fig. 1). To better characterize these tumors, we performed a global DNA methylation analysis and classified our cases according to the methylation classes of central nervous system tumors defined by Capper and colleagues (<https://www.molecularneuropathology.org/mnp> [3]). Moreover, we performed a *t*-distributed stochastic neighbor embedding (*t*-SNE) analysis including our case series as well as all cases published by Capper and colleagues ($n = 2801$, 82 tumor methylation classes ([3], Figure S1). Using the above-mentioned classifier, 7/12 tanycytic cases (58.3%) matched to one of the nine molecular ependymoma groups (Fig. 1, [23]).

Fig. 1 Clinical, histopathological, and molecular features of cases diagnosed as tancytic ependymoma ($n = 12$). *EPN* ependymoma, *Loc.* localisation, *ST* supratentorial, *PF* posterior fossa, *SP* spinal, *PR* pineal region, *Methyl. Class* methylation class defined by DNA methylation-based classification of central nervous system tumors (<https://www.molecularneuropathology.org/mnp>, [3]). *PFA* ependymoma, posterior fossa group A; *PFB* ependymoma, posterior fossa group B; *MPE* ependymoma, myxopapillary; *SP-EPN* ependymoma, spinal; *LGG*, *MYB* low-grade glioma, *MYB/MYBL1*; *Myxopap.* myxopapillary; *n.a.* not available

Case	1	2	3	4	5	6	7
Age [years]	10.4	40.1	15.0	45.8	80.7	45.8	28.9
Gender	f	f	f	f	f	m	m
Loc.	PR	SP, lumbar	PF	SP, cervical	SP, lumbar	SP, lumbar	SP, thoracic
Methyl. class	PFB	MPE	PFA	SP-EPN	MPE	MPE	SP-EPN
Classifier score	0.78	0.99	0.99	0.99	0.98	0.99	0.95
Histological reevaluation							
Histomorphology	tancytic/classic	tancytic/classic	tancytic/classic	tancytic	tancytic	tancytic/myxopap.	tancytic/classic
Immunohistochemistry	GFAP+, OLIG2-, H3K27me3+	GFAP n.a., OLIG2 n.a., Astra-	GFAP+, OLIG2 n.a., H3K27me3 n.a.	GFAP+, OLIG2-, Alcian-	GFAP+, OLIG2-, Alcian focally +	GFAP+, OLIG2-, Alcian focally +	GFAP+, OLIG2-, Alcian-
Integrated diagnosis	EPN, WHO °II	EPN, WHO °II	EPN, WHO °II	EPN, WHO °II	Myxopap. EPN, WHO °I	Myxopap. EPN, WHO °I	EPN, WHO °II

Histopathological diagnosis:
Tancytic ependymoma (n=12)



Case	8	9	10	11	12
Age [years]	17.7	15.6	15.6	50.2	53.4
Gender	m	f	f	m	f
Loc.	ST	ST	PF	SP, cervical	SP, lumbar
Methyl. class	no match	LGG, MYB	no match	no match	no match
Classifier score	<0.3	0.99	<0.3	<0.3	<0.3
Histological reevaluation					
Histomorphology	not available	angiocentric glioma pattern	low grade glioma with abundant calcifications	compatible with tancytic ependymoma	tancytic tumor with low cell density and hyalinized vessels
Immunohistochemistry	GFAP+, OLIG2-, p65-, MAP2C+, IDHR132H-	GFAP+, OLIG2-MAP2C+, CD34-, Synaptophysin-	GFAP+, OLIG2-, MAP2C+, p53-, H3K27me3+, ATRX+, IDHR132H-	GFAP+, OLIG2-, Alcian-, H3K27M-	GFAP+, OLIG2-Astra+, H3K27M-, Synaptophysin-
Integrated diagnosis	EPN, WHO °II	Angiocentric glioma, WHO °I	Low grade glioma, not classifiable	EPN, WHO °II	Myxopap. EPN, WHO °I

Tancytic ependymoma that matched to one of the nine known molecular ependymoma groups ($n = 7$) had a median age of 40.1 years (range 10.4–80.7) and were located spinally ($n = 5$, cases #2, 4, 5, 6, and 7) or in the posterior fossa/pineal region ($n = 2$, cases #1 and 3). Spinally located cases were attributed to the methylation classes of “ependymoma, myxopapillary” (MPE, $n = 3$) or “ependymoma, spinal” (SP-EPN, $n = 2$), whereas cases #1 and #3 were classified as “ependymoma, posterior fossa group B” (PFB) and “ependymoma, posterior fossa group A” (PFA), respectively (Fig. 1). The histomorphology of cases #1, 2, 3, and 7 was characterized by areas of tancytic morphology and classic morphology with characteristic ependymal pseudorosettes (Figs. 1, 2a–d). In case #1, sharply delineated islets with classic growth patterns were seen in between the predominantly tancytic-growing tumor (Fig. 2a). Cases

#4, 5, and 6 were characterized by tancytic morphology only (Fig. 2e–g). In summary, tumors with a histology of tancytic ependymoma and a match to any molecular ependymoma group occurred in pediatric and adult patients were located in the spinal cord and posterior fossa, and showed diverse molecular methylation patterns.

Among the cases not matching to any molecular ependymoma group ($n = 5$, 41.6%), case #9 was a supratentorial tumor in a 15.6-year-old female and was attributed to the methylation class “low grade glioma, MYB/MYBL1”. Upon re-evaluation, the histomorphology was indeed compatible with a low-grade astrocytoma with angiocentric growth pattern (Fig. 1, Supplementary Fig. 2, online resource). Details on the remaining 4/12 cases (33.3%) that did not match to any known methylation class based on a classifier score ≥ 0.5 are described in Fig. 1 and Supplementary Fig. 2 (online

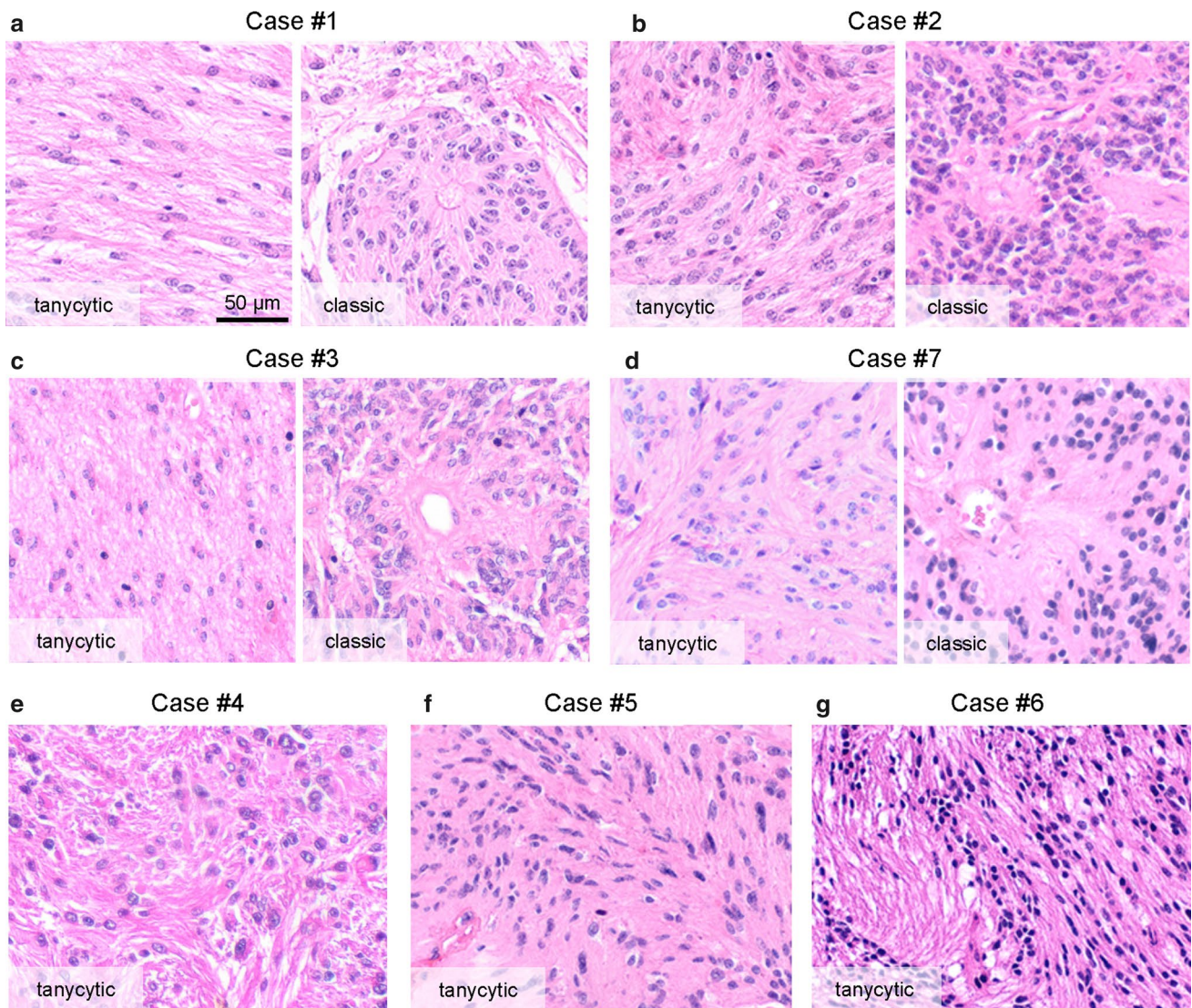


Fig. 2 Histomorphology of tancyctic ependymomas. **a–g** H&E stainings of all cases molecularly classified as ependymoma. Scale bar in **a**: 50 μ m for **a–g**. **a–d** Cases #1, 2, 3, and 7 showed areas with tancyctic morphology (left panels in **a–d**) and also classic morphology (right panels in **a–d**). The tancyctic parts showed moderate cellularity with elongated tumor cells and oval nuclei. Cases #2 and #7 displayed tumor cells arranged in interlacing fascicles (**b**, **d**, left panels). Areas with classic morphology displayed the characteristic ependymal pseu-

dosettes and tumor cells showed round nuclei with finely dispersed chromatin (right panels in **a–d**). In case 1, sharply delineated islets with classic growth patterns were visible in between the predominantly tancyctic-growing tumor (**a**). **e–g** Cases #4, 5, and 6 were characterized by tancyctic morphology only. Tumor cell nuclei in case #4 displayed also subtle pleomorphism and several tumor cells showed abundant eosinophilic or granular cytoplasm (**e**)

resource). These tumors were localized supratentorially ($n = 1$), in the posterior fossa ($n = 1$), or in the spinal cord ($n = 2$). The additionally performed *t*-SNE analysis (Supplementary Fig. 1, online resource) showed that cases #11 and #12 clustered closely to different spinal ependymoma groups (EPN, SP, and SUBEPN, SP). However, the two other tancyctic ependymomas without a classifier match did not cluster together or close to ependymomas, arguing against a common molecular group build by these four tumors without a classifier match (Supplementary Fig. 1, online resource).

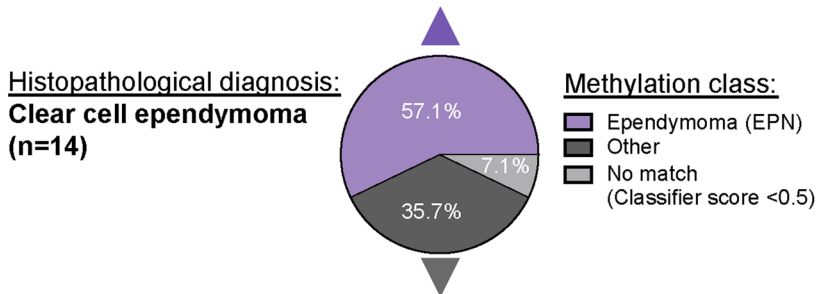
Clear cell ependymoma

Clear cell ependymomas ($n = 14$) had a median age of 12.7 years (range 0.9–56.9) with a female-to-male ratio of 1.3:1 (Fig. 3). DNA methylation revealed that 8/14 cases (57.1%) matched to one of the ependymoma subgroups (Fig. 3, [5]), whereas 6/14 (42.8%) did not.

Clear cell ependymomas (75%) with a molecular match to ependymoma subgroups were attributed to the methylation class “ependymoma, RELA fusion” (RELA, 6/8 cases

Fig. 3 Clinical, histopathological, and molecular features of cases diagnosed as clear cell ependymoma ($n = 14$). *EPN* ependymoma, *Loc.* localisation, *ST* supratentorial, *PF* posterior fossa, *SP* spinal. *Methyl. Class* methylation class defined by DNA methylation-based classification of central nervous system tumors (<https://www.molecularneuropathology.org/mnp>, [3]). *PFA* ependymoma, posterior fossa group A, *RELA* ependymoma, *RELA* fusion, *SP-EPN* ependymoma, spinal, *LGG*, *DNT* low-grade glioma, dysembryoplastic neuroepithelial tumor, *PLEX*, *PED B* plexus tumor, subclass pediatric B, *neurocytoma* central neurocytoma, *PTPR, A* papillary tumor of the pineal region group A, *PTPR, B* papillary tumor of the pineal region group B, *n.a.* not available, *n.d.* not done

Case	13	14	15	16	17	18	19	20
Age [years]	3.7	0.9	13.3	51.7	17.8	11.5	2.4	37.6
Gender	f	m	f	m	m	m	m	f
Loc.	ST	ST	ST	ST	ST	ST	PF	SP, thoracic
Methyl. class	RELA	RELA	RELA	RELA	RELA	RELA	PFA	SP-EPN
Classifier score	0.99	0.99	0.99	0.90	0.99	0.99	0.89	0.97
Histological reevaluation								
Histomorphology	Clear cell morphology						Microcystic morphology	
Immunohistochemistry	GFAP+, OLIG2-, p65+						GFAP+, OLIG2-, H3K27me3-	GFAP+, OLIG2-, Alcian-
RELA fusion	+	+	+	+	n.a.	+	-	n.a.
Integrated diagnosis	RELA-fusion-positive EPN, WHO °III						Anapl. EPN, WHO °III	EPN, WHO °II



Case	21	22	23	24	25	26
Age [years]	12.2	7.5	6.1	30.8	56.9	21.9
Gender	f	f	f	f	f	m
Loc.	ST	ST	PF	ST	ST	ST
Methyl. class	no match	LGG, DNT	PTPR, B	PTPR, A	PLEX, PED B	Neurocytoma
Classifier score	0.30	0.85	0.99	0.98	0.54	0.99
Histomorphology	compatible with clear cell ependymoma	compatible with DNT	cell dense, clear cell tumor, no papillary structures or pseudorosettes	clear cell tumor without papillary structures	clear cells with accentuated cell boundaries and nuclei free vascular spaces, no plexus tissue	typical appearance of central neurocytoma with calcifications
Immunohistochemistry	GFAP+, OLIG2-, p65+	GFAP+, OLIG2+, p65-, NeuN-, CD34-, S100+, Synapto-	GFAP+, OLIG2-, p65-, Synapto-, Vim+, Keratin+, H3K27me3+, H3K27M-	GFAP+, p65-, OLIG2-, Vim+, Keratin+, Synapto-	GFAP+, OLIG2+, p65-, Vim+, EMA-, NeuN-, Keratin-, ATRX+, IDHR132H-, Synapto-	Synapto+, NeuN+, p65-
RELA fusion	+	n.d.	n.d.	n.d.	n.d.	n.d.
Integrated diagnosis	RELA-fusion-positive EPN, WHO °III	DNT, WHO °I	Papillary tumor of the pineal region, WHO °III	Papillary tumor of the pineal region, WHO °II	High grade glioma, not classifiable	Central neurocytoma WHO °II

(#13–18), Fig. 3). Clear cell ependymomas classified as *RELA* were all localized supratentorially, had a median age of 12.4 years (range 0.9–51.7) and a female-to-male ratio of 1:2 (Fig. 3). These cases showed a similar histomorphology with quite densely packed, monomorphic tumor cells with narrow clear cytoplasm (clear cell appearance) intercepted by mostly thin and branching capillaries (Fig. 4a–f). In contrast, cases #19 and 20 showed more variable cell density and a microcystic appearance (Fig. 4g, h). These tumors were localized in the posterior fossa (case #19) or spinal

cord (case #20) and matched to the “PFA” and “SP-EPN” group, respectively. In summary, molecularly confirmed ependymomas with typical clear cell appearance all fell into the molecular group of *RELA*-fusion-positive ependymoma.

Next, we asked whether clear cell ependymomas may form a distinct molecular cluster within the molecular group of *RELA*-fusion-positive ependymoma. We compared global methylation patterns of *RELA*-fusion-positive clear cell ependymoma (*RELA*, clear cell morphology (CCM), $n = 6$) with *RELA*-fusion-positive ependymomas

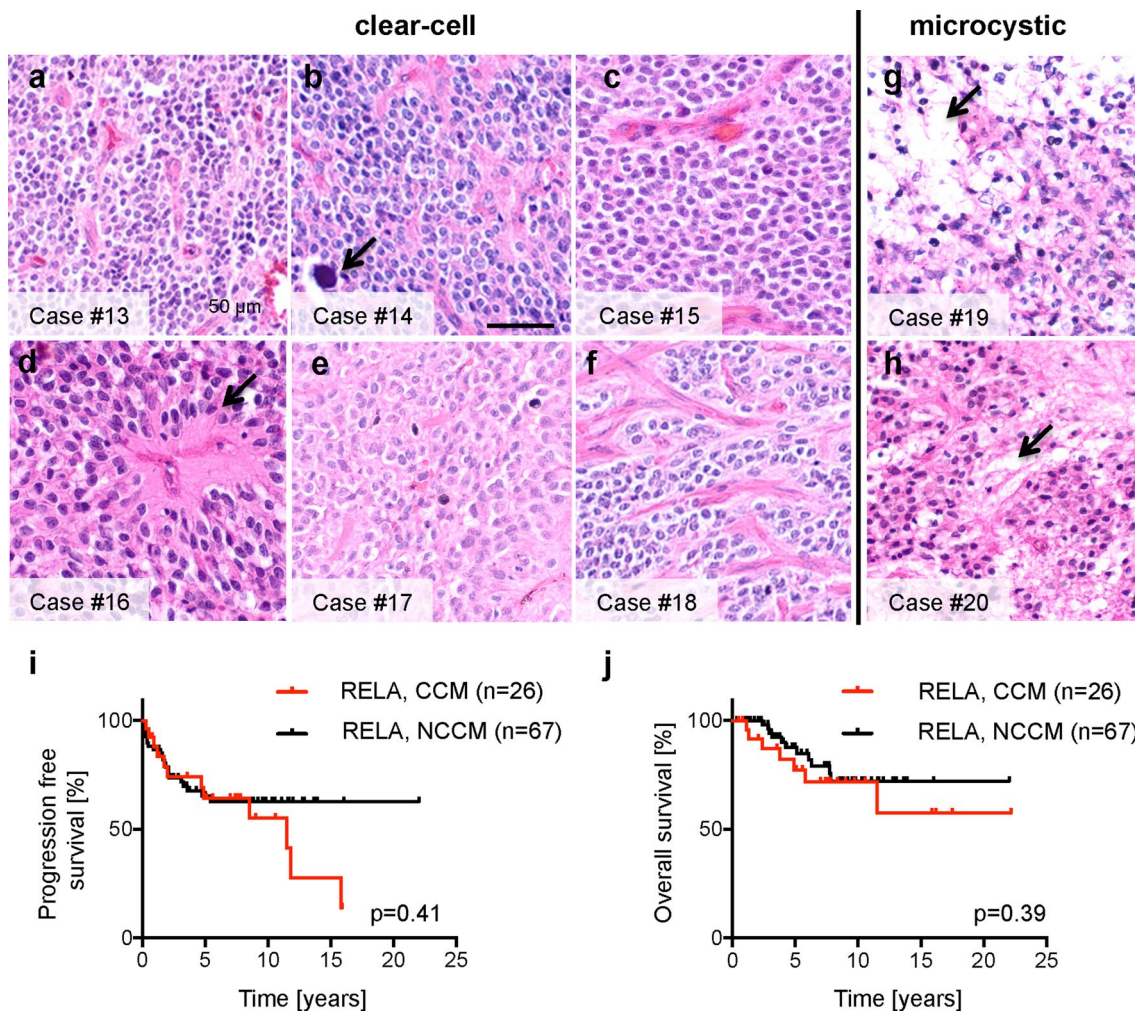


Fig. 4 Histomorphology and survival of clear cell ependymoma cases. **a–h** H&E stainings of all cases molecularly classified as ependymoma. Scale bar in **a**: 50 μ m for **a–h**. **a–f** Cases #13, 14, 15, 16, 17, and 18 showed quite densely packed, monomorphic tumor cells with narrow clear cytoplasm intercepted by mostly thin and branching capillaries. Arrow in **b** shows a calcification. Sometimes pseudorosettes were implied (arrow in **d**). **g, h** Cases #19 and 20 showed a more variable cell density and a microcystic appearance

(arrows in **g, h**). Sometimes, tumor cells with irregular and clumpy appearing clear cytoplasm were seen. (**i, j**) Kaplan–Meier survival analyses of RELA ependymomas comparing cases with ($n=26$) or without clear cell morphology ($n=67$). Overall survival (**i**) and progression-free survival (**j**) did not differ significantly. *RELA, CCM* RELA ependymoma, clear cell morphology, *RELA, NCCM* RELA-fusion-positive ependymoma, no clear cell morphology

that did not display clear cell morphology (RELA, no clear cell morphology (NCCM), $n=65$, Supplementary Fig. 2, online resource). Only 4 significantly differentially methylated CpG sites were detected (FDR < 0.1) and RELA, CCM did not cluster separately based on the most differentially methylated CpG sites (Supplementary Fig. 4a, Supplementary Table 1, online resource). In a *t*-SNE analysis, RELA, CCM cases did not cluster together and located scattered among RELA, NCCM cases (Supplementary Fig. 4b, online resource). Finally, RELA, CCM and RELA, NCCM cases showed similar chromosomal alterations, including losses on chromosomes 3 and 9, as published previously ([23, 26], Supplementary Fig. 4c, online resource).

We then questioned if RELA, CCM were clinically distinct from RELA, NCCM cases. We, therefore, compared the RELA, CCM and RELA, NCCM cases within the HIT-MED study cohort. RELA, CCM cases represented 6.9% of RELA cases (5/72 cases). Patient age of HIT study cohort cases did not significantly differ between RELA, CCM and RELA, NCCM cases (median age_{RELA, CCM} = 11.5 years (range_{RELA, CCM} 0.9–17.8 years, $n=5$) and median age_{RELA, NCCM} = 5.8 years (range_{RELA, NCCM} 0.4–18.6 years, $n=67$, $p=0.49$). The female-to-male ratio was 0.67:1 for RELA, CCM cases and 0.58:1 for RELA, NCCM cases. Next, we performed a Kaplan–Meier survival analysis of RELA ependymomas and included a series of previously

published clear cell ependymomas molecularly defined as RELA by p65 immunostaining and reverse transcription PCR for *C11ORF95-RELA* fusions ($n=20$, [9]). RELA, CCM ($n=26$) did not differ significantly from RELA, NCCM ($n=67$) concerning progression-free survival and overall survival ($p=0.41$ and $p=0.39$, respectively, Fig. 4i, j). Both groups showed a 10 year survival rate of 72% (Fig. 4j). In conclusion, our data indicate that RELA, CCM do not significantly differ from RELA, NCCM cases concerning global DNA methylation and clinical parameters.

Among the clear cell cases not matching to any molecular ependymoma group, case #21 did not match to any known methylation class (classifier score ≤ 0.3). However, this case displayed a histomorphology well compatible with clear cell ependymoma (Supplementary Fig. 3, online resource), showed nuclear p65-positivity and an *RELA*-fusion transcript (Fig. 3). Other cases matched to the methylation classes “low grade glioma, dysembryoplastic neuroepithelial tumor” (case #22), “papillary tumor of the pineal region group A” (case #24), “papillary tumor of the pineal region group B” (case #23), “plexus tumor, subclass pediatric B” (case #25), and “central neurocytoma” (case #26). Upon re-evaluation, histology was well compatible with molecular diagnoses in all cases. Details on histomorphology and additional analyses of all cases are shown in Figs. 3 and 4 and Supplementary Fig. 3 (online resource).

Papillary ependymoma

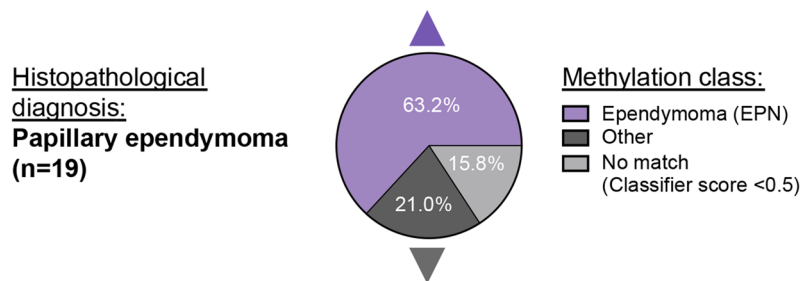
Finally, we analyzed cases with a primary diagnosis of papillary ependymomas ($n=19$). These tumors had a median age of 36.4 years (range 6.3–78.1) with a female-to-male ratio of 0.9:1 (Fig. 5). Classification according to the methylation classifier [8] attributed 12/19 cases (63.2%) to one of the molecular ependymoma groups (Fig. 5, [23]). These cases fell into the PFB group ($n=6$), the MPE group ($n=4$), the RELA group ($n=1$), and the SP-EPN group ($n=1$, Fig. 5). Reanalysis of histomorphology of these cases revealed three different growth patterns that we defined as truly “papillary” (finger-like extensions lined by epithelial-like surfaces with smooth boundaries), as “pseudo-papillary” (discohesive monomorphic tumor cells lined around vessels) or as “trabecular” (trabecular growth pattern with abundant cysts lined by a smooth epithelial-like surface, Figs. 5 and 6a–f). 4/6 pseudo-papillary growing tumors were classified as MPE. These cases displayed hyalinized blood vessels and a myxoid matrix becoming apparent with Alcian blue staining. All tumors displaying a bona fide papillary growth pattern matched to the methylation class PFB (cases #27, 28, 30, 31, and 32, Figs. 5, 6a–c). All cases were GFAP-positive and OLIG2-negative and 4/5 cases displayed sustained nuclear H3K27me3 staining. Case #27, a tumor in 33 years with a high PFB classifier score, showed a loss of H3K27me3, a

feature that was reported to be associated with PFA ependymomas typically occurring in children [22]. PFB cases had a median age of 33.3 years. Except for one case (#28) that was localized supratentorially and had a rather low classifier score of 0.54, all cases arose in the posterior fossa (Fig. 5). Radiological data to reevaluate the location of case #28 were not available, but this case showed sustained nuclear H3K27me staining and no nuclear p65 accumulation in tumor cells, supporting the molecular diagnosis. 4/6 cases (67%) with pseudo-papillary growth pattern matched to the MPE group (Figs. 5, 6d). These cases had a median age of 41.4 years and 3/4 cases were localized in the spinal cord. Of note, case #33 was located supratentorially, but showed a typical myxoid stroma around blood vessels (Fig. 6d). The spinally located cases barely displayed a myxoid component. Finally, case #38 with trabecular growth pattern was localized in the spinal cord and was classified as “ependymoma, spinal” (Fig. 6f). In conclusion, a true papillary growth pattern was strongly associated with the PFB group.

Next, we asked whether PFB cases with papillary growth ($n=5$) were molecularly distinct from PFB cases with non-papillary growth ($n=15$). We detected 2406 significantly differentially methylated CpG sites (FDR < 0.1 , Supplementary Table 1, online resource) when comparing papillary PFB cases with non-papillary PFB cases, and papillary PFB cases formed a separate cluster in an unsupervised hierarchical cluster analysis (FDR < 0.1 , delta beta value ≥ 0.2 shown, Fig. 6g). Within the group of PFB ependymomas, five subtypes had been previously described [5] and we questioned whether these subtypes might be associated with histomorphological patterns. We, therefore, re-analyzed the Cavalli data set and performed a *t*-SNE plot including our papillary PFB and non-papillary PFB cases (Supplementary Fig. 6a, online resource). Papillary PFB ($n=5$) and non-papillary PFB cases ($n=15$) located scattered among PFB cases of the five subtypes, indicating no significant association of histomorphology and subtypes (Supplementary Fig. 6a, online resource). Finally, copy number analyses revealed that non-papillary PFB had a frequent gain on Chromosome 11 that was not seen in papillary PFB cases (Supplementary Fig. 6b, online resource). Other chromosomal alterations were common in both groups, including losses on chromosomes 6, 10, 16, and 17, consistent with previously published data [5]. In conclusion, PFB cases with papillary growth showed significant differences concerning DNA methylation when compared to PFB cases without papillary growth.

Among the cases not clustering to ependymoma based on DNA methylation, cases #39, 44, and 45 were localized in the spine and did not match to any known subgroup (classifier score < 0.3). The other tumors were classified as “plexus tumor, subclass pediatric B” (case #40), “low grade glioma, dysembryoplastic neuroepithelial tumor” (case #41), and “CNS high grade neuroepithelial tumor with MN1

Case	27	28	30	31	32	33	34	35	36	29	37	38
Age [years]	33.3	14.4	37.0	55.6	24.6	39.5	44.1	16.0	42.6	78.1	6.3	36.4
Gender	m	m	f	m	f	f	m	f	m	f	m	m
Loc.	PF	ST	PF	PF	PF	ST	SP, lumbar	SP, lumbar	SP, lumbar	PF	ST	SP, cervical
Methyl. class	PFB	PFB	PFB	PFB	PFB	MPE	MPE	MPE	MPE	PFB	RELA	SP-EPN
Classifier score	0.95	0.54	0.99	0.99	0.99	0.99	0.63	0.98	0.99	0.99	0.99	0.99
Histological reevaluation												
Histo-morphology	true papillary growth pattern					pseudo-papillary growth pattern						trabecular
Immunohistochemistry	GFAP+, OLIG2-, Keratin-, H3K27me3-	GFAP+, p65-, OLIG2-, Keratin-, H3K27me3+	GFAP+, OLIG2-, Keratin focally+, H3K27me3+	GFAP+, OLIG2-, Keratin-, H3K27me3+	GFAP+, OLIG2-, Keratin-, H3K27me3+	GFAP+, OLIG2-, Alcian+, p65-	GFAP+, OLIG2-, Alcian+	GFAP+, OLIG2-, Alcian+	GFAP+, OLIG2-, Alcian+	GFAP+, OLIG2-, H3K27me3+	GFAP-, OLIG2-, p65+	GFAP+, OLIG2-, Alcian-, K27M-
RELA fusion	n.d.	n.d.	n.d.	n.d.	n.d.	n.d.	n.d.	n.d.	n.d.	n.d.	+	n.d.
Integrated diagnosis	EPN, WHO °II	EPN, WHO °II	EPN, WHO °II	EPN, WHO °II	EPN, WHO °II	Myxopap. EPN, WHO °I	Myxopap. EPN, WHO °I	Myxopap. EPN, WHO °I	Myxopap. EPN, WHO °I	EPN, WHO °II	RELA-fusion-pos. EPN, WHO °III	EPN, WHO °II

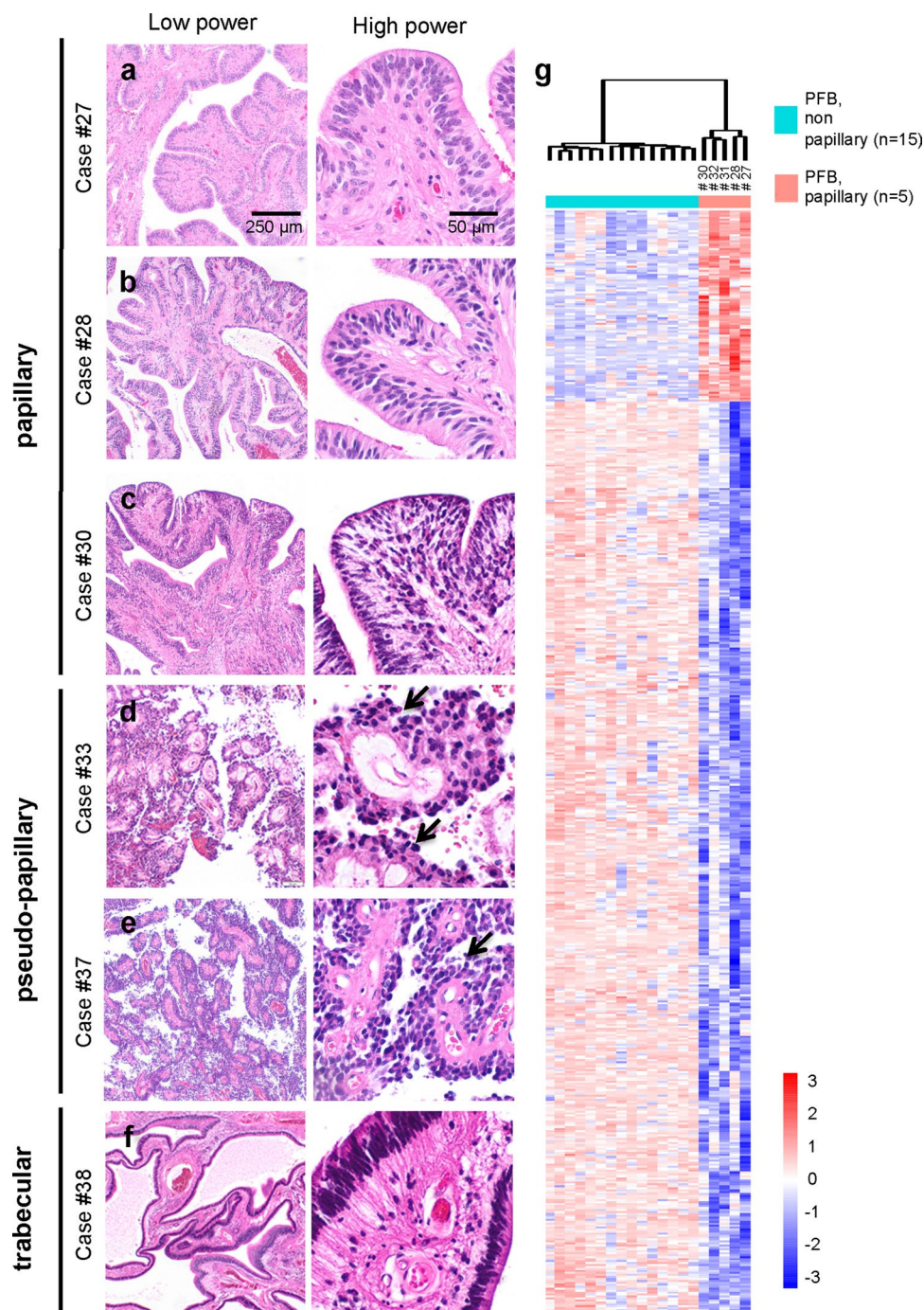


Case	39	40	41	42	43	44	45
Age [years]	18.2	60.0	16.6	36.0	11.0	38.0	56.6
Gender	m	f	f	m	f	m	f
Loc.	SP, thoracic	PF	ST	SP, thoracic	ST	SP, thoracic	SP, lumbar
Methyl. class	no match	PLEX, PED B	LGG, DNT	HGNET, MN1	HGNET, MN1	no match	no match
Classifier score	<0.3	0.5	0.53	0.98	0.99	<0.3	<0.3
Histological reevaluation							
Histo-morphology	cell dense tumor with some perivascular accentuation and dis-coherence resulting in a pseudo-papillary picture	well compatible with plexus tumor	highly vascularized tumor, nuclei-free areas and circular arrangement of tumor cells around vessels, dehiscence with pseudopapillary appearance	cell dense tumor with hyalinized vessels and dis-coherence resulting in a pseudo-papillary picture	cell dense tumor with hyalinized vessels and dis-coherence resulting in a pseudo-papillary picture	abundant trabecular structures resembling ependymal canals, no pseudo-rosettes	tumor cell nests within a myxoid matrix, no pseudo-rosettes, focal pseudo-papillary pattern
Immunohisto-chemistry	GFAP+, Keratin-, MAP2C focally+, NFP-, Vim+, no further stains available	GFAP+, OLIG2-, Keratin+	GFAP+, OLIG2+, Vim+, Keratin-, NeuN+, MAP2C+, p65-, S100+, EMA+, Synapto+	GFAP+, OLIG2+, Vim+	GFAP-, OLIG2-, Vim+, p65-	GFAP+, OLIG2-, H3K27M-, Alcian-	GFAP+, OLIG2-, Alcian+, ATRX+, H3K27M-, Keratin-, Brachyury-
MN1 alteration (FISH)	n.d.	n.d.	n.d.	-	+	-	-
Integrated diagnosis	High grade glioma, not classifiable	Choroid plexus papilloma, WHO °I	Papillary glioneuronal tumor (WHO °I)	Astroblastoma	Astroblastoma	EPN, WHO °II	Unclassifiable tumor

Fig. 5 Clinical, histopathological, and molecular features of cases diagnosed as papillary ependymoma (n=19). EPN ependymoma, Loc. localisation, ST supratentorial, PF posterior fossa, SP spinal, Methyl. Class methylation class defined by DNA methylation-based classification of central nervous system tumors (<https://www.molecularneuropathology.org/mnp> [3]). PFB ependymoma, posterior fossa

group B, RELA ependymoma, RELA fusion, MPE ependymoma, myxopapillary, SP-EPN ependymoma, spinal, PLEX, PED B plexus tumor, subclass pediatric B, LGG, DNT low-grade glioma, dysembryoplastic neuroepithelial tumor, HGNET, MNI CNS high-grade neuroepithelial tumor with MN1 alteration, Myxopap. myxopapillary, n.a. not available, n.d. not done

Fig. 6 Histomorphology and DNA methylation of papillary ependymoma cases. **a–f** Representative H&E stainings of cases molecularly classified as ependymoma. Scale bar in **a** left panel (low magnification): 250 μ m for left panels in **a–f**. Scale bar in **a** right panel (high magnification): 50 μ m for right panels in **a–f**. **a–c** Cases #27, 28, and 30 as examples for ependymomas with a true papillary growth pattern. These cases showed finger-like extensions lined by epithelial-like surfaces with smooth boundaries. This epithelial-like layer lacked a basement membrane, but showed cuboidal cells with fibrillary processes directed down to a vascular core. **d, e** Cases #33 and 37 as examples for ependymomas with pseudo-papillary growth pattern. Discohesive monomorphic tumor cells line around vessels. Note that boundaries are irregular (arrows in **d, e**). **f** Case #38 showed a trabecular growth pattern with abundant cysts lined by a smooth epithelial-like surface. **g** Unsupervised hierarchical clustering analysis of PFB ependymoma, based on 559 significantly differentially methylated CpG sites (FDR < 0.1, delta beta value \geq 0.2) comparing papillary morphology with non-papillary morphology. Details on all 2406 significantly differentially methylated CpG sites are listed in supplementary Table 1 (online resource). *PFB* ependymoma, posterior fossa group B



alteration” (cases #42 and 43). Histological re-evaluation in an integrated setting confirmed the plexus tumor in case #40 and identified two astroblastomas (cases #42 and 43, Fig. 5, Supplementary Fig. 5, online resource). Details on these cases and on all other cases not matching to ependymoma groups are delineated in Fig. 5 and Supplementary Fig. 5 (online resource).

Overall, the neuropathological re-evaluation of ependymoma variants, including histological and molecular data, confirmed the initial diagnosis in 55.6% of cases. Diagnosis

or WHO grade was changed in 35.6% of cases, whereas 8.9% of cases were not classifiable (Table 1).

Discussion

We analyzed a series of 45 ependymoma variants that were diagnosed as papillary, tanyctic, or clear cell ependymoma and carefully re-evaluated histological features, gathered epidemiological and clinical data, and performed

Table 1 Reclassification of ependymoma variants

Integrated diagnosis	Tanycytic EPN	Clear cell EPN	Papillary EPN	Total number	% of cases
Ependymoma—same WHO grade	7	9	9	25	55.6
Ependymoma—change of WHO grade	3	0	4	7	15.6
Other entity	1	4	4	9	20
Not classifiable	1	1	2	4	8.9
Total number of cases	12	14	19	45	100

DNA methylation profiling. Given the rarity of such variants, a thorough histological description and visualization may first of all add to the sparse knowledge of neuropathology textbooks on these tumors. Furthermore, the current and upcoming integration of molecular data into the WHO classification of brain tumors requires a careful correlation between molecular features and histomorphology, which we have performed here for ependymoma variants. This may not only be useful in circumstances, where histology remains the only available diagnostic tool for whatever reason. A well-educated view on the histology of a brain tumor with supposedly tanycytic, clear cell, or papillary features may also encourage the neuropathologist to consider a wider spectrum of differential diagnoses that have emerged within our series 45 cases. Of note, based on global DNA methylation, 18/45 cases did not match to any methylation class of ependymoma with some of them showing specific similarities to low-grade gliomas, plexus tumors, neurocytomas, pineal tumors, or neuroepithelial tumors with *MNI* alteration. The majority of these cases were localized supratentorial (10/18, 55%). Previous studies have reported a high discordance rate of histological and molecular diagnosis in up to 23% supratentorial ependymomas [10, 27], indicating that supratentorial ependymomas in general may be a challenging diagnosis.

In the integrated neuropathological review, diagnosis was changed for 35.6% of cases, which clearly exceeds overall discordance rates between histology and DNA methylation-based classification of brain tumors, which were reported to be around 12% in general [3]. Our results show that low-grade gliomas, plexus tumors, neurocytomas, pineal tumors, or neuroepithelial tumors with *MNI* alteration are important differential diagnoses.

Consistent with the previous reports [30, 31], the majority of analyzed tanycytic ependymomas that were molecularly confirmed to be ependymomas were located in the spinal cord (71.4%). They displayed irregular fascicles of variable width and cell density, a pattern similar to low-grade astrocytic tumors. Some of these cases harbored small areas with transition to classic ependymal histology, but most tumors showed a distinct morphology with moderate cellularity and elongated tumor cells that were arranged in interlacing fascicles. The possible lack of any classic ependymal

morphology (e.g., perivascular pseudorosettes) remains—in our opinion—challenging in diagnosing this tumor. This was reflected by a huge fraction of cases (41.6%) that were not classified as ependymomas using the DKFZ classifier. Tanycytic ependymomas that, based on global methylation patterns, were classified as ependymomas fell into diverse molecular ependymoma groups, arguing against a common molecular background and a common cellular origin. Two cases were classified as “ependymoma, spinal”, a molecular tumor class associated with *NF2* mutations [23], and this is consistent with single case reports describing *NF2* mutations in tanycytic ependymomas [6, 17]. Other tanycytic cases were classified as “ependymoma, myxopapillary”, which was confirmed upon neuropathological re-evaluation in 2/3 cases. MPE cases were all localized within the lumbar spine or filum terminale, where single tanycytic cases have previously been reported [25]. In summary, tanycytic ependymoma does not represent a homogeneous molecular group, but is a histological feature observed in molecularly diverse ependymomas.

Consistent with the previous reports, clear cell ependymomas showed perinuclear halos mimicking an oligodendroglioma phenotype or resembling central neurocytoma. Two cases of our series had to be reclassified as DNT and neurocytoma after careful re-evaluation [19]. Two cases turned out to be papillary tumors of the pineal region, highlighting this entity as another important differential diagnosis. Most clear cell ependymomas showed thin branching capillaries with sparsely implied pseudorosettes. In our series, clear cell ependymomas with typical histomorphology were all found supratentorially and fell into the methylation class of *RELA*-EPN. In line with this, a pathological activation of nuclear factor- κ B signaling has been previously reported in clear cell ependymoma cases [9]. Case #21 that did not show a match to ependymoma based on DNA methylation still showed a histomorphology well compatible with clear cell ependymoma. In addition, this case located with *RELA* cases in a *t*-SNE analysis (Figure S1). The tumor finally displayed nuclear p65 accumulation via immunohistochemistry and an *RELA*-fusion, resulting in the integrated diagnosis of an *RELA*-fusion-positive ependymoma (WHO grade III). Comparing clear cell and non-clear cell *RELA*-EPN, no

significant differences concerning DNA methylation, epidemiology, and prognosis have been detected, supporting the idea that a clear cell ependymoma might clinically behave like any other *RELA*-fusion-positive ependymoma.

Papillary ependymomas are extremely rare tumors and only sporadic case reports exist, describing tumors with diverse histomorphology and spinal or supratentorial localization [7, 12, 28]. We describe a set of 19 tumors diagnosed as papillary ependymomas. However, seven of these (36.8%) were not classified as ependymomas based on DNA methylation profiling with HGNET, MN1 ($n=2$) being a relevant differential diagnosis. Those tumors molecularly confirmed to be ependymomas displayed diverse growth patterns that we defined as “papillary”, “trabecular”, or “pseudo-papillary”. In line with the description in the WHO classification, we considered a truly papillary growth pattern only upon presence of finger-like extensions lined by a layer of cuboidal epithelial-like cells [18]. This epithelial-like layer shows fibrillary processes directed down to a vascular core and lacks a basement membrane. The surface presented smooth boundaries. One case (#38) displayed the “trabecular” pattern, lacking finger-like projections, but showing abundant cysts lined by a smooth epithelial-like surface. Case #44 that did not show a match in the methylation classifier displayed a trabecular growth pattern similar to case #38. This case clustered to SP-EPN in the *t*-SNE analysis (Figure S1) and showed an immunoprofile well compatible with an ependymoma. Finally, the “pseudo-papillary” pattern was more variable, but showed discohesive monomorphic tumor cells lined around vessels. Boundaries of pseudopapillae were irregular. Applying the strict rule to only consider a true papillary growth pattern as a papillary ependymoma did result in a very clear association of papillary ependymomas with the PFB methylation class. This is in line with the relatively old age of respective patients and may indicate that papillary ependymomas go along with a better prognosis compared to the majority of posterior fossa ependymoma accounting for the PFA methylation group [23].

Of note, 7/45 cases in our cohort were reclassified as myxopapillary ependymomas in an integrated diagnostic setting, which resulted in a change of WHO grading. Except for case #33, all these cases were localized in the lumbar spine. 3/12 tanycytic ependymomas were reclassified as myxopapillary ependymomas, and this is well in line with the fibrillary tanycytic pattern that was described in myxopapillary ependymomas [2]. Four myxopapillary ependymomas had initially been diagnosed as papillary ependymoma, but all displayed a pseudo-papillary growth pattern. Myxopapillary ependymomas initially diagnosed as tanycytic or papillary ependymomas shared the lack of classic ependymal pseudorosettes, had characteristic hyalinized vessels and a—sometimes only focally present—myxoid matrix that was detected with Alcian blue or Astra staining. These results

highlight the histopathological diversity of myxopapillary ependymomas and indicate that the differential diagnosis of a myxopapillary ependymoma should be considered—even in the absence of an apparent myxoid stroma—in any possible ependymoma case arising in the lumbar spine.

For the eight cases that did not match to any of the brain tumor classes known by the DKFZ classifier, multiple scenarios appear possible. First, technical reasons might have hampered a specific match, although we included only cases with sufficiently high tumor cell content in the analyzed tissue as well as a good DNA quality and sufficient quantity. Second, molecularly uncommon tumors can occur in patients harboring tumor predisposing germline mutations. In this context, it is worth mentioning that case #10 had a Gorlin–Goltz syndrome and harbored a *PTCH1* germline mutation. The quite old age of many other affected patients in our cohort argues against possible additional underlying tumor predisposition syndromes. Finally, some tumors with uncommon histology that were diagnosed as histological ependymoma variants might belong to rare, so far undefined, molecularly distinct tumor classes that are not represented in the reference data set. Nevertheless, our integrated diagnosis of cases with no match resulted in *RELA*-fusion-positive ependymoma, WHO °III ($n=1$), ependymoma, WHO °II ($n=3$), and myxopapillary ependymoma ($n=1$), whereas four tumors were not classifiable.

Of the cases that, based on DNA methylation, were reclassified into other tumor entities ($n=10$), a thorough neuropathological workup confirmed the molecular diagnosis in eight cases. This is in line with reported reclassifications after careful molecular workup [14, 29] underlining the value of DNA-methylation-based classification as a helpful tool in neuropathology. For two cases (#25, 41), the result of DNA methylation-based classification could not be confirmed. The latter cases showed a low classifier score (<0.54) albeit high tumor content was assured. Case #25 showed a histopathology that could not be classified into any of the known WHO defined entities, whereas case #41 was rediagnosed as a papillary glioneuronal tumor.

Taken together, our analyses contribute to the knowledge on histological ependymoma variants by showing data about epidemiology, localization, and histology of such cases. Furthermore, we provide global DNA methylation data and correlate these data with clinical, histological, and genetic findings. Finally, we increase the awareness for differential diagnoses that need to be considered when assuming ependymoma. Although we did not detect a distinct DNA methylation pattern associated with tanycytic ependymomas, it is important to be aware of the tanycytic variant as a possible feature of posterior fossa or spinal ependymomas. Here, the differential diagnosis of an ependymoma should be considered in cases resembling low-grade astrocytoma-like tumors that lack typical ependymal pseudorosettes. Furthermore,

we confirmed that the histomorphological pattern of clear cell ependymoma is tightly related to the molecular group of RELA-fusion-positive ependymoma. Finally, a true papillary growth pattern was associated with the molecular group of posterior fossa B ependymoma.

Acknowledgements We thank Anne Reichstein for her dedication and excellent technical support concerning the DNA-methylation analyses. We also thank Ulrike Rumpf, Hannelore Junker-Polzin, Carolina Janko, Tasje Lempertz, and Celina Liza Soltwedel for excellent technical support with tissue sections and stainings. J.N. was supported by the Else-Kröner Fresenius Stiftung and the UKE Nachwuchsförderung. This project was generously funded by the Gert and Susanna Mayer Stiftung. U.S. was supported by the Fördergemeinschaft Kinderkrebszentrum Hamburg.


References

- Aryee MJ, Jaffe AE, Corrada-Bravo H, Ladd-Acosta C, Feinberg AP, Hansen KD et al (2014) Minfi: a flexible and comprehensive bioconductor package for the analysis of inffinium DNA methylation microarrays. *Bioinformatics* 30:1363–1369. <https://doi.org/10.1093/bioinformatics/btu049>
- Burger PCSB, Kleinschmidt-DeMasters B, Tihan T, Rodriguez F et al (2016) Diagnostic pathology: neuropathology. Diagnostic pathology series, 2nd edn
- Capper D, Jones DTW, Sill M, Hovestadt V, Schrimpf D, Sturm D et al (2018) DNA methylation-based classification of central nervous system tumours. *Nature* 555:469–474. <https://doi.org/10.1038/nature26000>
- Capper D, Stichel D, Sahm F, Jones DTW, Schrimpf D, Sill M et al (2018) Practical implementation of DNA methylation and copy-number-based CNS tumor diagnostics: the Heidelberg experience. *Acta Neuropathol* 136:181–210. <https://doi.org/10.1007/s00401-018-1879-y>
- Cavalli FMG, Hubner JM, Sharma T, Luu B, Sill M, Zapotocky M et al (2018) Heterogeneity within the PF-EPN-B ependymoma subgroup. *Acta Neuropathol* 136:227–237. <https://doi.org/10.1007/s00401-018-1888-x>
- Cepeda S, Hernandez-Lain A, Munarriz PM, Martinez Gonzalez MA, Lagares A (2014) Spinal tanycytic ependymoma associated with neurofibromatosis type 2. *Clin Neuropathol* 33:311–314. <https://doi.org/10.5414/NP300704>
- Chaudhuri PM, Chakrabarty D, Chaudhuri S, Chatterjee U (2019) Papillary ependymoma of the spinal cord: a case report with summary of prior published cases. *Asian J Neurosurg* 14:223–226. https://doi.org/10.4103/ajns.AJNS_250_17
- Ebert C, von Haken M, Meyer-Puttlitz B, Wiestler OD, Reifenberger G, Pietsch T et al (1999) Molecular genetic analysis of ependymal tumors. NF2 mutations and chromosome 22q loss occur preferentially in intramedullary spinal ependymomas. *Am J Pathol* 155:627–632. [https://doi.org/10.1016/S0002-9440\(10\)65158-9](https://doi.org/10.1016/S0002-9440(10)65158-9)
- Figarella-Branger D, Lechapt-Zalcman E, Tabouret E, Junger S, de Paula AM, Bouvier C et al (2016) Supratentorial clear cell ependymomas with branching capillaries demonstrate characteristic clinicopathological features and pathological activation of nuclear factor-kappaB signaling. *Neuro Oncol* 18:919–927. <https://doi.org/10.1093/neuonc/now025>
- Fukuoka K, Kanemura Y, Shofuda T, Fukushima S, Yamashita S, Narushima D et al (2018) Significance of molecular classification of ependymomas: C11orf95-RELA fusion-negative supratentorial ependymomas are a heterogeneous group of tumors. *Acta Neuropathol Commun* 6:134. <https://doi.org/10.1186/s40478-018-0630-1>
- Gatta G, Botta L, Rossi S, Aareleid T, Bielska-Lasota M, Clavel J et al (2014) Childhood cancer survival in Europe 1999–2007: results of EUROCARE-5—a population-based study. *Lancet Oncol* 15:35–47. [https://doi.org/10.1016/S1470-2045\(13\)70548-5](https://doi.org/10.1016/S1470-2045(13)70548-5)
- Grajkowska W, Matyja E, Pronicki M, Daszkiewicz P, Roszkowski M, Perek D et al (2009) Papillary ependymoma with unique superficial cortical location: immunohistochemical and ultrastructural studies. A case report. *Folia Neuropathol* 47:354–361
- Hovestadt VZM (2017) conumee: Enhanced copy-number variation analysis using Illumina DNA methylation arrays. R package version 1.9.0
- Hwang EI, Kool M, Burger PC, Capper D, Chavez L, Brabetz S et al (2018) Extensive molecular and clinical heterogeneity in patients with histologically diagnosed CNS-PNET treated as a single entity: a report from the children’s oncology group randomized ACNS0332 trial. *J Clin Oncol*. <https://doi.org/10.1200/jco.2017.76.4720>
- Kilday JP, Rahman R, Dyer S, Ridley L, Lowe J, Coyle B et al (2009) Pediatric ependymoma: biological perspectives. *Mol Cancer Res* 7:765–786. <https://doi.org/10.1158/1541-7786.MCR-08-0584>
- Kolde R (2019) pheatmap: Pretty Heatmaps. R package version 1.0.12
- Kuga Y, Ohnishi H, Kodama Y, Takakura S, Hayashi M, Yagi R et al (2014) Cerebral and spinal cord tanycytic ependymomas in a young adult with a mutation in the NF2 gene. *Neuropathology* 34:406–413. <https://doi.org/10.1111/neup.12109>
- Louis DN, Ohgaki H, Wiestler OD, Ellison DW, Figarella-Branger D, Perry A et al (2016) WHO classification of tumours of the central nervous system (revised 4th edn). Lyon, IARC
- Min KW, Scheithauer BW (1997) Clear cell ependymoma: a mimic of oligodendroglioma: clinicopathologic and ultrastructural considerations. *Am J Surg Pathol* 21:820–826
- Morris TJ, Butcher LM, Feber A, Teschendorff AE, Chakravathy AR, Wojdacz TK et al (2013) ChAMP: 450 k chip analysis methylation pipeline. *Bioinformatics* 30:428–430. <https://doi.org/10.1093/bioinformatics/btt684>
- DNACopy: DNA copy number data analysis (2019)
- Pajtler KW, Wen J, Sill M, Lin T, Orisme W, Tang B et al (2018) Molecular heterogeneity and CXorf67 alterations in posterior fossa group A (PFA) ependymomas. *Acta Neuropathol* 136:211–226. <https://doi.org/10.1007/s00401-018-1877-0>
- Pajtler KW, Witt H, Sill M, Jones DT, Hovestadt V, Kratochwil F et al (2015) Molecular classification of ependymal tumors across all CNS compartments, histopathological grades, and age groups. *Cancer Cell* 27:728–743. <https://doi.org/10.1016/j.ccell.2015.04.002>
- Parker M, Mohankumar KM, Punchihewa C, Weinlich R, Dalton JD, Li Y et al (2014) C11orf95-RELA fusions drive oncogenic NF-kappaB signalling in ependymoma. *Nature* 506:451–455. <https://doi.org/10.1038/nature13109>
- Radhakrishnan N, Nair NS, Hingwala DR, Kapilamoorthy TR, Radhakrishnan VV (2012) Tanycytic ependymoma of filum terminale: a case report. *Clin Neurol Neurosurg* 114:169–171. <https://doi.org/10.1016/j.clineuro.2011.09.017>
- Rickert CH, Korshunov A, Paulus W (2006) Chromosomal imbalances in clear cell ependymomas. *Mod Pathol* 19:958–962. <https://doi.org/10.1038/modpathol.3800614>
- Sasaki A, Hirato J, Hirose T, Fukuoka K, Kanemura Y, Hashimoto N et al (2019) Review of ependymomas: assessment of consensus in pathological diagnosis and correlations with genetic profiles and outcome. *Brain Tumor Pathol* 36:92–101. <https://doi.org/10.1007/s10014-019-00338-x>

28. Stark AM, Hugo HH, Nabavi A, Mehdorn HM (2009) Papillary ependymoma WHO Grade II of the aqueduct treated by endoscopic tumor resection. *Case Rep Med* 2009:434905. <https://doi.org/10.1155/2009/434905>
29. Sturm D, Orr BA, Toprak UH, Hovestadt V, Jones DT, Capper D et al (2016) New brain tumor entities emerge from molecular classification of CNS-PNETs. *Cell* 164:1060–1072. <https://doi.org/10.1016/j.cell.2016.01.015>
30. Tao X, Dong J, Hou Z, Hao S, Zhang Q, Wu Z et al (2017) The clinical features and surgical outcomes of intracranial tanyctic ependymomas: a single-institutional experience. *J Neurooncol* 134:339–347. <https://doi.org/10.1007/s11060-017-2531-8>
31. Tao X, Hou Z, Hao S, Zhang Q, Wu Z, Zhang J et al (2017) The clinical features and surgical outcomes of spinal cord tanyctic ependymomas: a report of 40 cases. *World Neurosurg* 106:60–73. <https://doi.org/10.1016/j.wneu.2017.06.111>
32. Upadhyaya SA, Robinson GW, Onar-Thomas A, Orr BA, Billups CA, Bowers DC et al (2019) Molecular grouping and outcomes of young children with newly diagnosed ependymoma treated on the multi-institutional SJYC07 trial. *Neuro Oncol*. <https://doi.org/10.1093/neuonc/noz069>
33. Wickham H (2016) *ggplot2: elegant graphics for data analysis*. Springer, New York

Publisher's Note Springer Nature remains neutral with regard to jurisdictional claims in published maps and institutional affiliations.

Affiliations

Julia E. Neumann¹ · Michael Spohn^{2,15} · Denise Obrecht³ · Martin Mynarek³ · Christian Thomas⁴ · Martin Hasselblatt⁴ · Mario M. Dorostkar^{5,6} · Annika K. Wefers^{7,8,9} · Stephan Frank¹⁰ · Camelia-Maria Monoranu¹¹ · Arend Koch¹² · Hendrik Witt^{9,13,14} · Marcel Kool^{9,13} · Kristian W. Pajtler^{9,13,14} · Stefan Rutkowski³ · Markus Glatzel¹ · Ulrich Schüller^{1,3,15} 

¹ Institute of Neuropathology, University Medical Center Hamburg-Eppendorf, Hamburg, Germany

² II. Medizinische Klinik und Poliklinik, University Medical Center Hamburg-Eppendorf, Hamburg, Germany

³ Department of Pediatric Hematology and Oncology, University Medical Center Hamburg-Eppendorf, Hamburg, Germany

⁴ Institute of Neuropathology, University Hospital Münster, Münster, Germany

⁵ Center for Neuropathology, Ludwig-Maximilians-University, Munich, Germany

⁶ German Center for Neurodegenerative Diseases, Munich, Germany

⁷ Department of Neuropathology, Institute of Pathology, University Hospital, Heidelberg and Clinical Cooperation Unit Neuropathology, German Cancer Consortium (DKTK), German Cancer Research Center (DKFZ), Heidelberg, Germany

⁸ Clinical Cooperation Unit Neuropathology, German Cancer Consortium (DKTK), German Cancer Research Center (DKFZ), Heidelberg, Germany

⁹ Hopp Children's Cancer Center Heidelberg (KiTZ), Heidelberg, Germany

¹⁰ Institute of Pathology, University of Basel, Basel, Switzerland

¹¹ Department of Neuropathology, Institute of Pathology, University of Würzburg, Würzburg, Germany

¹² Department of Neuropathology, Charité-Universitätsmedizin Berlin, Corporate Member of Freie Universität Berlin, Humboldt-Universität zu Berlin, and Berlin Institute of Health, Berlin, Germany

¹³ Division of Pediatric Neuro-Oncology, German Cancer Research Center (DKFZ), German Cancer Consortium (DKTK), Heidelberg, Germany

¹⁴ Department of Pediatric Oncology and Hematology, University Hospital Heidelberg, Heidelberg, Germany

¹⁵ Research Institute Children's Cancer Center Hamburg, Hamburg, Germany